Conformal MIMO Ultra-Wideband Antenna Design for High-Speed Wireless Telemetry in Capsule Endoscopy Systems

Liu Chang, *Student Member, IEEE,* Amjad Iqbal, *Member, IEEE,* Abdul Basir, *Member, IEEE,* Roy B. V. B. Simorangkir, *Member, IEEE,* Ismail Ben Mabrouk, *Senior Member, IEEE*

***Abstract*—This article presents a novel ultra-wideband (UWB) antenna for multiple-input-multiple-output (MIMO) operations in wireless capsule endoscopy (WCE) applications. The design is capable of supporting high channel capacity for real-time transmission and addressing the frequency detuning effect. Thanks to the conformal meander structure, the design efficiently utilizes the inner wall space of the capsule, achieving both compactness and wideband operation. The proposed MIMO antenna consists of two elements, each occupying a volume of 7.192 mm^3. The experimental measurements are performed inside a minced pork meat. The antenna covers a bandwidth range from 0.61 GHz to 1.51 GHz, achieving a fractional bandwidth (FBW) of 84.91% and a peak gain of -30.4 dBi. An isolation level greater than 20 dB is maintained, indicating low mutual coupling between MIMO antenna elements. The specific absorption rate (SAR) is evaluated to be 0.0202 W/kg at a transmitted power of -16 dBm, and the link margin is calculated to be 20 dB at a distance of 2 meters. Therefore, the proposed bio-telemetry system confirms its suitability for safe and high data rate communications.**

***Index Terms*—Wireless capsule endoscopy (WCE), conformal antenna, ultra-wideband (UWB), multiple-input-multiple-output (MIMO), industrial scientific medical (ISM) band, link margin.**

I. Introduction

OVER the past several years, the demand for implantable medical devices (IMDs), including wireless capsule endoscopy (WCE) [1], pacemakers [2], and intracranial pressure monitors [3], have significantly increased, due to the expanding role in health monitoring and diagnosis systems [4]. IMDs are particularly important for monitoring and collecting physiological parameters inside the human body over extended periods. These devices transmit vital data to the receiver, assisting doctors for better diagnosis. WCE, for instance, is introduced to address limitations of traditional wired endoscopes, such as blind spots within the Gastrointestinal (GI) tract, by enabling a comprehensive examination of the entire GI tract.

Despite advancements in WCE research work, the technology still faces several challenges. Ensuring high-channel capacity for high-data-rate transmission of images and videos to cloud servers is a complicated task [5]–[7]. Moreover, antenna frequency detuning poses a significant challenge, due to the complex electromagnetic (EM) properties of the human body's tissues and fluids along the GI tract [7], [8]. This issue is further aggravated by the dynamic movements and changes in the patient's posture. These variations can alter the effective impedance seen by the antenna, resulting in a shift in the antenna's operating frequency [9]. In [10]–[12], researchers adopt long-arm spiral and open-slotted designs to adjust the electrical length, and enhance the bandwidth. However, it should be noted that the designs in [10]–[12] are single-input-single-output (SISO) topologies. SISO systems provide lower data throughput and are more susceptible to signal fading, leading to potential drops in reliability and performance. To address these challenges, the combination of both MIMO and UWB technologies has emerged as a promising solution. This fusion provides higher data rates, improved robustness against multipath fading, and effective frequency detuning mitigation [13]–[16]. The relationship between channel capacity, bandwidth, and MIMO antenna elements could be presented in (1) [17],

$$C = BW \log_2(det(I_N + \frac{P_T}{\sigma^2 M} H H^H)) \tag{1}$$

where C is channel capacity, BW presents the channel bandwidth, M is the number of independent channels, P_T is the equally distributed input power among the elements, σ^2 is the noise power, I_N is the N $\times$ N identity matrix, H is the complex channel matrix, and H^H is the conjugate transpose of H.

Recent studies in [18]–[21] have discussed the integration of technologies such as UWB or MIMO for implantable antenna application. In [18], a compact two-module MIMO antenna system utilizing a grounded meander resonator and open slots achieved significant miniaturization (5.35 mm $\times$ 6.2 mm $\times$ 0.12 mm), offering a FBW of 13.1% (320 MHz) and 28 dB isolation. In [19], authors introduced a patch antenna based on a circular structure with symmetrical arc-shaped slots, achieving a FBW of 33.9% (355 MHz - 500 MHz) and compact dimensions (0.13 $\times$ π $\times$ 5.65^2 mm^3). In [20], a spiral symmetry structure embedded into the ground is used to achieve a bandwidth from 320 MHz to 460 MHz, with a FBW of 25.9% and a modest volume (22 mm $\times$ 12 mm $\times$ 0.635 mm). A quad-element MIMO antenna system detailed in [21] comprises semi-circular meander radiators, achieving a FBW of 38.26% (355 MHz - 523 MHz) with dimensions of

Manuscript received 9 March 2024. (Corresponding author: Liu Chang). This work is supported by the Royal Society under Newton International Fellowship (Grant Number: NIF\R1\221500). Liu Chang, Amjad Iqbal, Roy B. V. B. Simorangkir, and Ismail Ben Mabrouk are with the Department of Engineering, Durham University, Durham DH1 3LE, U.K., Abdul Basir is with the Department of Engineering, Tampere University, Hervanta 33720 Tampere, Finland (e-mail: chang.liu5@durham.ac.uk; abdul.basir@tuni.fi; amjad730@gmail.com; roy.b.simorangkir@durham.ac.uk; ismail.benmabrouk@durham.ac.uk).

13.5 mm × 13.5 mm × 0.13 mm.

However, these reported MIMO antenna systems employ planar configurations. Such planar antenna structures occupy considerable space inside the capsule, limiting the available volume for other essential components. Conformal designs, presented in [22] and [23], have been introduced to address space constraints for WCE applications. In [22], researchers presented a dual planner helical radiator achieving a FBW of 15.1% (2.26 GHz - 2.63 GHz) with an antenna size of 34.65 mm^3. In [23], authors utilized a conformal-rectangular patch antenna combined with a curved slotted structure, attaining a FBW of 12.63% (0.84 GHz - 0.96 GHz) and a size of 29.91 mm^3. Nevertheless, while these innovative conformal designs aim to minimize space occupation, they often do not achieve UWB characteristics and face a trade-off between size and bandwidth. This paper presents a novel conformal dual-element MIMO antenna system for WCE applications. The MIMO antenna elements exhibit UWB characteristics, from 0.61 GHz to 1.51 GHz with 84.91% FBW. This design has a volume of 30.5 mm × 15 mm × 0.04 mm placed on the 11 mm × 26 mm inner wall of the capsule. The proposed antenna design offers (1) high data transmission and (2) effectively mitigates frequency detuning without compromising on the overall antenna performance or device compactness. To the best of the authors' knowledge, the proposed MIMO antenna model achieves the widest bandwidth among existing MIMO antennas, along with the smallest reported size to date.

II. Design Methodology

The WCE components outlined in this paper are depicted in Fig. 1(a). It comprises two antenna elements, four batteries, a camera, sensors, and a Printed Circuit Board (PCB). The all above components are encapsulated in a 3D-printed capsule, made from bio-compatible Polyimide (ε_r = 3.5, tanδ = 0.008). Fig. 1(b) illustrates the structure of the two antenna element model in its unfolded condition. The material will bend along the capsule's inner wall and be attached at the feeding point to create a loop. Fig. 1(c) displays the proposed WCE model from various viewing angles. This design utilizes a Polyimide substrate with 0.04 mm thickness to achieve compactness and flexibility. The antennas form a minimal volume of 14.384 mm^3. Eight holes are evenly distributed on the substrate between the two antennas to further enhance the impedance matching. This configurations can reduce the local effective permittivity of the substrate to optimize the impedance matching [24].

A. Simulation Environment

The proposed antenna model is designed within a phantom model and optimized in a heterogeneous human body model, as illustrated in Fig. 2. Initially, we used a phantom model represented by a three-layered cylinder configuration in the High Frequency Structure Simulator (HFSS), as depicted in Fig. 2(a). The cylinder, consists of muscle, fat, and skin. The permittivity and dielectric dissipation factor of these tissues vary with frequency [25]. In the next step, the proposed antennas are optimized in a heterogeneous human model in

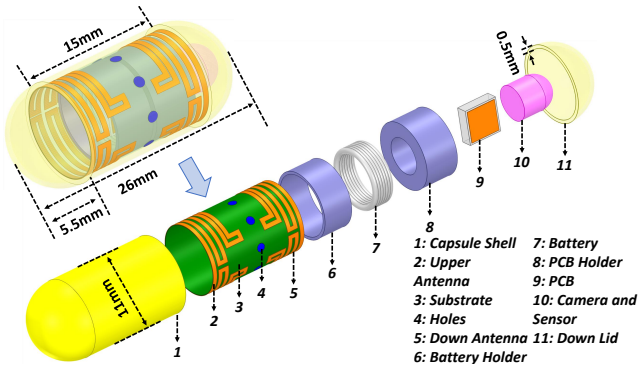

(a)

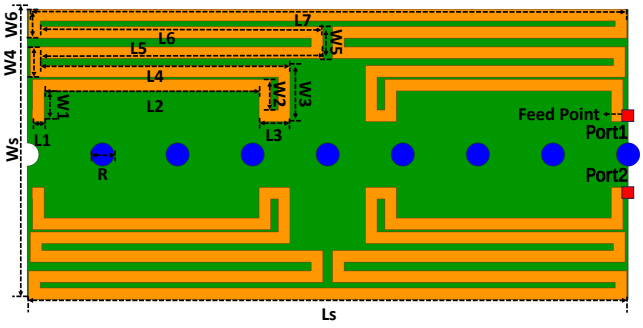

(b)

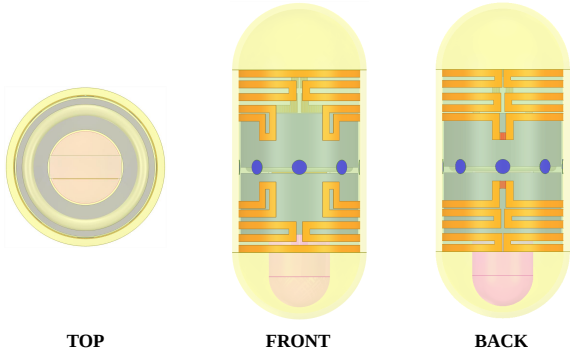

(c)

Fig. 1: (a) The proposed WCE system partial view. (b) Planar antenna structure diagram. (c) Top, front, and back view of WCE model. The geometrical dimension of planar antenna: L_S = 30.5, W_S = 15, L_1 = 0.618, L_2 = 11.088, L_3 = 1.594, L_4 = 12.799, L_5 = 14.499, L_6 = 14.585, L_7 = 30.87, W_1 = 1.585, W_2 = 1.585, W_3 = 2.9, W_4 = 1.5625, W_5 = 2.9, W_6 = 1.4875, R = 0.6 (Unit: mm).

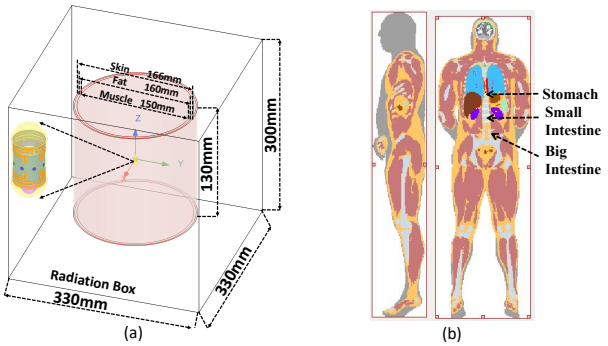

(a) (b)

Fig. 2: Setup of MIMO system simulation. (a) Three-layered cylinder phantom model simulation. (b) Heterogeneous human model simulation.

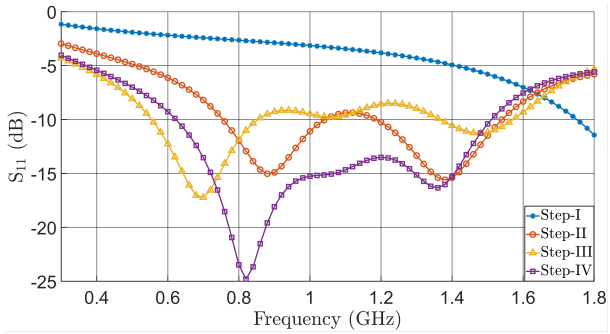

(a)

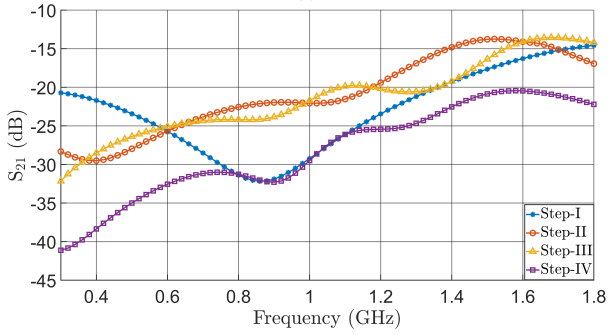

(b)

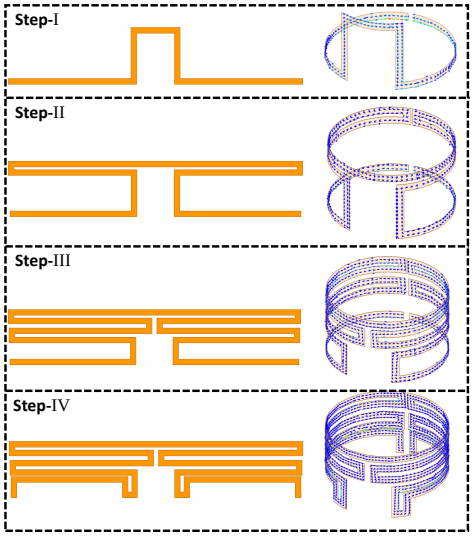

(c)

Fig. 3: (a) The S_{11} with different steps. (b) The S_{21} with different steps. (c) The current distribution with different steps.

CST Studio Suite (CST), as shown in Fig. 2(b). The proposed MIMO antenna system is simulated at different regions of the GI tract.

B. Evolution Steps

In this study, the proposed antenna model goes through four iterative steps to obtain the desired results. Fig. 3(a) and (b) show the S-parameters under different steps. As shown in Fig. 3(c), Step-I demonstrates that when the antenna consists of a single metal wire with a single bend, its resonant frequency stands at 2.25 GHz. The isolation level between the two antennas is 14 dB. Step-II involves bending and folding the

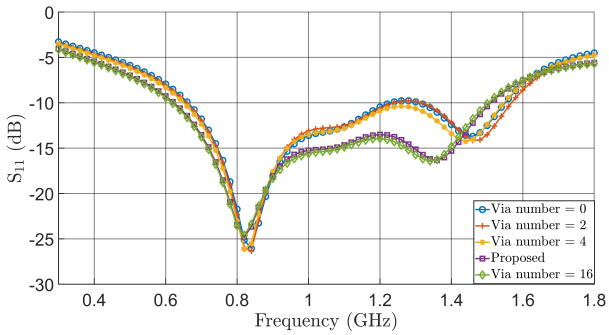

(a)

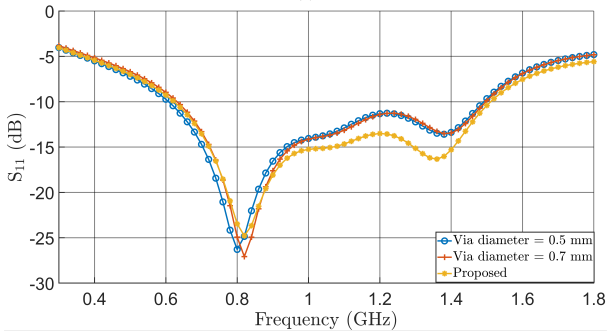

(b)

Fig. 4: (a) Holes numbers effect. (b) Holes diameter effect.

antenna to extend its electrical length. This extension allows current to flow along the newly created radiating components on the surface. As a result, the resonant frequency is reduced. Furthermore, the mirror structure modifies the original design, enhancing the bandwidth. The antenna's operating frequency band covers 915 MHz. However, the impedance matching between 1 GHz and 1.2 GHz remains poor and the isolation is about 13 dB. Step-III involves designing a new mirror-symmetric structure to introduce an additional operating frequency. Accordingly, the antenna is operating at three frequencies of 0.67 GHz, 1.3 GHz, and 1.45 GHz resulting in an improved overall bandwidth. However, the antenna's self-inductance leads to an impedance mismatch from 0.9 to 1.35 GHz. Therefore, in Step IV, a reverse vector current technique [26] is implemented to decrease the self-inductance and enhance impedance matching in this band. The bandwidth of the fully optimized antenna ranges from 0.61 to 1.51 GHz, with a FBW of 84.91% and an isolation level better than 20 dB.

C. The Influence of Holes

The presence of holes between the antennas effectively reduces the local permittivity on the substrate. The lower permittivity enables EM waves to propagate more rapidly within the substrate. This technique permits antennas of identical physical lengths to support a broader frequency range and enhance impedance matching [24].

Fig. 4(a) and (b) show the impact of varying holes number and size on S_{11}. It is noted that the reflection coefficient in the 1.2-1.4 GHz frequency range consistently exceeds -10 dB in the absence of holes between the two antennas.

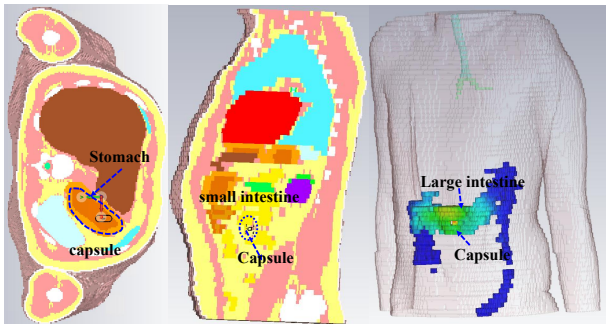

Fig. 5: The robustness validation in stomach, small, and big intestine.

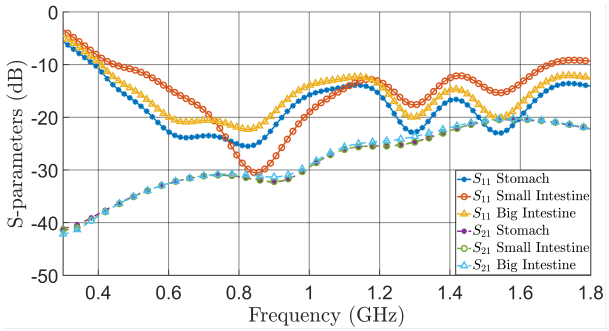

Fig. 6: The S-parameters at stomach, small, and big intestine.

The antenna's S_{11} exhibit minimal change when two holes are arranged between antennas. The reflection coefficient falls below -10 dB when 4 holes are integrated. S_{11} between 1.2 and 1.4 GHz frequency band is further reduced to -13.5 dB using 8 holes arrangement. Additionally, the effect of 16 holes on the S_{11} is investigated. However, the impact is determined to be negligible. Consequently, an arrangement with 8 holes is adopted.

Furthermore, the effect of holes diameter on S_{11} is investigated. Fig.4(b) illustrates the direct effect on S_{11} when the holes diameters are 0.5 mm, 0.6 mm (proposed), and 0.7 mm. Holes with diameter of 0.6 mm are found to achieve the best performance in terms of bandwidth.

D. S-Parameters at Various GI Tract Locations

The human body comprises various biological tissues, each possessing different electromagnetic properties, including dielectric constant and conductivity. The antenna's impedance matching is affected by the surrounding tissue. In Fig. 5, the proposed MIMO antenna system is implanted at various locations within a CST heterogeneous human model to simulate realistic scenarios. Fig. 6 shows the S_{11} and S_{21} results when the antenna model is implanted at the stomach, small, and big intestine. The proposed antenna demonstrates UWB characteristics, ranging from 0.4 to 1.8 GHz, when positioned in the stomach. After relocating the antennas from the stomach to the small intestine, the bandwidth narrows to 0.5-1.7 GHz frequency range. However, the lowest reflection coefficients are reached when the antenna moves to the big intestine section. The operating range remains from 0.5 GHz to 1.8 GHz. Regardless of the antenna position inside the GI tract, it consistently maintains UWB characteristics and covers the ISM band.

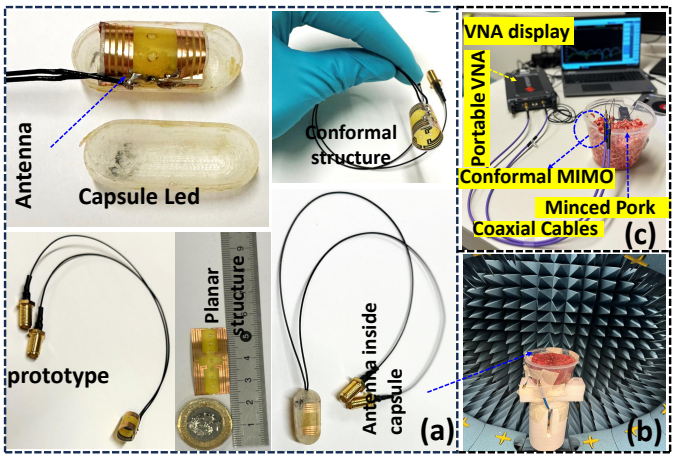

Fig. 7: (a) The fabricated antenna prototype before and after encapsulating. (b) Setup for Measuring Radiation Patterns. (c) Setup for Measuring S-Parameters.

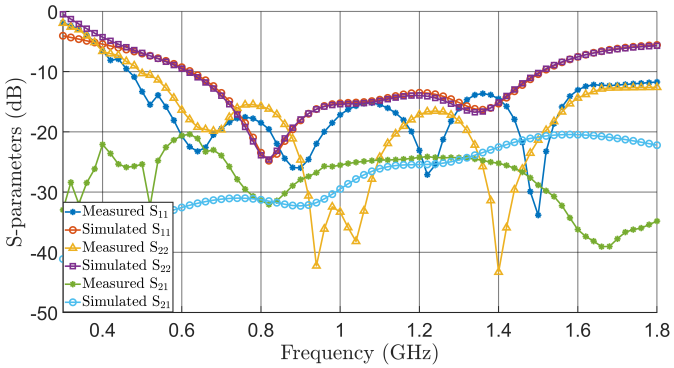

Fig. 8: Comparison of simulated and measured S-parameters.

III. Results and Analysis

The proposed antenna design is fabricated using the specified Polyimide substrate to validate the simulated results. Fabricated antennas prototype are shown in both planar and conformal configurations in Fig. 7(a). For the antenna's S-parameter and radiation pattern measurements, the entire assembly is then immersed in minced pork, serving as a tissue-equivalent material for the human digestive system.

A. S-Parameters

The proposed antenna's S-parameters are measured using a Keysight P9374A portable Vector Network Analyzer (VNA), with the antenna elements connected via coaxial cables. A comparison between the simulated and measured S-parameters is shown in Fig. 8. The simulated results indicate a working frequency range from 0.61 GHz to 1.51 GHz, a fractional bandwidth (FBW) of 84.91%, and an isolation level better than 20 dB between the two antennas. The measured results demonstrate that the suggested antenna maintains a reflection coefficient below -10 dB across a slightly wider frequency range, from 0.5 GHz to 1.8 GHz, with a similar isolation

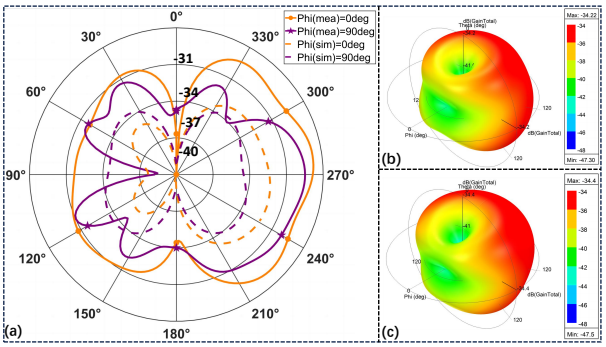

Fig. 9: (a) Comparison of simulation and measurement radiation pattern at 915MHz. (b) 3D radiation pattern for antenna 1 at 915MHz. (c) 3D radiation pattern for antenna 2 at 915MHz.

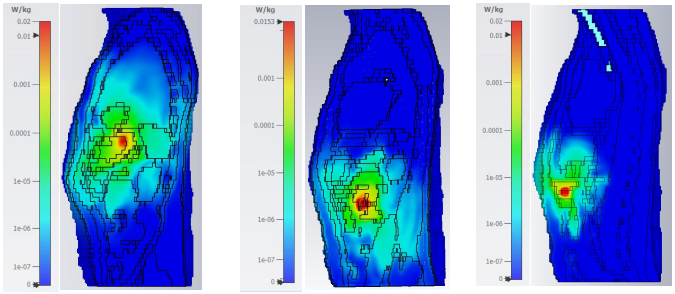

Fig. 10: 10-g averaged SAR distribution at 915MHz when antennas are placed in stomach, small intestine, and big intestine.

level. Discrepancies between these results can be attributed to several factors related to the manual assembly and integration process. One of the main challenges arises from the use of the thin Polyimide substrate, which needs to be conformed to the capsule structure during integration. The conforming process may introduce slight deformations, such as substrate stretching or compression, which can affect the antenna's performance, leading to discrepancies between the simulation and measurement. Additionally, potential variations in the positioning and alignment of the antennas and other elements within the capsule and inconsistencies in the manual soldering of the coaxial cables to the antenna elements may also contribute to the observed discrepancies. Furthermore, differences in the dielectric properties between the heterogeneous human model used in the simulation and the actual minced pork used in measurements may also play a role. Despite these factors, the overall performance of the proposed antenna remains consistent with the simulated results, demonstrating its ultra-wideband characteristics and reliability, which confirms its suitability for WCE applications.

B. Radiation Pattern and Gain

The fabricated antenna prototype is measured in an anechoic chamber while immersed in minced pork to validate the antenna radiation performance in the target application, as depicted in Fig. 7(b). One port of the MIMO antennas connects to the spectrum analyzer, and the second port terminates with a 50 Ω load. A high-gain horn antenna is used as the transmitting antenna, positioned one meter away from the proposed antenna. The incoming power at the proposed antenna is captured with a 1° angular resolution.

Fig. 9(a) presents the simulated and measured 2D radiation patterns at ϕ values of 0° and 90° at 915 MHz. The simulated radiation pattern exhibits a peak gain of -34 dBi, while the measured peak gain is -30.4 dBi. This discrepancy can be attributed to the factors discussed earlier. Despite these differences, the main lobe of the radiation pattern spans from θ = 30° to 150° and from θ = 210° to 330° in both simulated and measured results. The 3D radiation patterns of the proposed antenna are illustrated in Fig. 9(b) and (c) when antenna 1 and antenna 2 are excited, respectively. Both antennas exhibit similar radiation patterns, with the main lobe oriented along the θ direction (0° - 180°) and the ϕ direction (90° - 270°). This characteristic ensures that the antenna maintains high gain over a wide angular range, enabling efficient transmission and reception of signals through the human body, which is crucial for reliable communication in WCE applications.

C. SAR Evaluation

In WCE applications, the capsule containing the antenna system is ingested by the patient and travels through the GI tract, making it crucial to ensure the EM radiation exposure is within safe limits to prevent potential harm to the patient. SAR is a vital parameter for evaluating the absorption of EM waves by the human body. The IEEE C95.1-2019 standard specifies that the maximum 10 gram averaged SAR should below than 2 W/kg to ensure patient safety [27]. To comprehensively assess the SAR performance of the proposed antenna, numerical simulations are analyzed using the human body model. The capsule with the integrated antenna is implanted within the stomach, small intestine, and large intestine in the simulations to account for various positions of the capsule during its transit through the GI tract. The simulations are performed with an input power of 25 μW, following the guidelines set by ITU-R RS.1346 [28] for implantable medical devices.

Fig. 10 shows the SAR analysis carried out at the operating frequency of 915 MHz. As can be seen, the calculated 10-g averaged SAR values for all scenarios are significantly lower than the 2 W/kg limit specified by the IEEE C95.1-2019 standard. The highest SAR value, 0.0202 W/kg, is observed when both antennas are excited simultaneously, and the capsule is located within the stomach and large intestine. The SAR values for single antenna excitation and small intestine placement are found to be 0.0101 W/kg and 0.0153 W/kg, respectively. These results consistently demonstrate that the proposed antenna system maintains a low level of EM exposure, ensuring patient safety for operation within the GI tract, making it a suitable candidate for WCE applications.

D. Link Margin Analysis

The primary objective of wireless capsule endoscopy is the transmission of photographic and video data from the human digestive to an external receiver. Throughout this period, to maintain the effective transmission of biological data by telemetry equipment to the receiver point, the parameter

This article has been accepted for publication in IEEE Transactions on Antennas and Propagation. This is the author's version which has not been fully edited and content may change prior to final publication. Citation information: DOI 10.1109/TAP.2024.3411703

TABLE I
RELEVANT VARIABLE FOR LM ANALYSIS

Specification	Variable	Value
Operation Frequency (GHz)	f	0.915
Implantable Antenna Gain (dBi)	G_t	-34
Transmitted Power (dBm)	P_t	-16
Transmitter Mismatching Losses (dB)	L_t	0
Distance (m)	d	0-20
Path Loss (dB)	L_p	Distance dependent
Path Loss Exponent	γ	1.5
Shadowing Effect (dB)	S_e	4
Receiving Antenna Gain (dBi)	G_r	2.1
Receiver Mismatching Loss (dB)	L_r	0
Feeding Losses (dB)	L_f	2
Polarization Mismatching Losses (dB)	PL	0.6

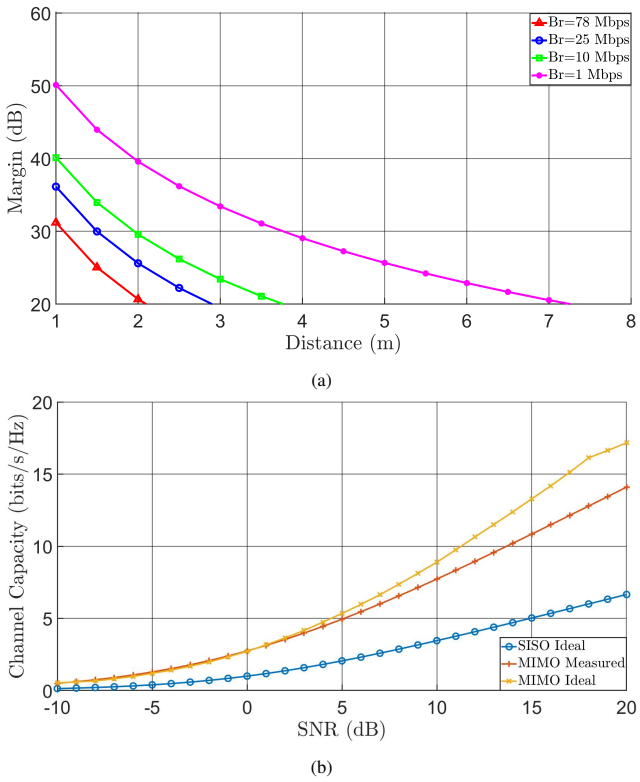

Fig. 11: (a) The Link Margin of the proposed antenna model at 915 MHz. (b) The channel capacity of SISO (ideal), MIMO (measured), MIMO (ideal).

Link Margin (LM) is important. This parameter assesses the backup signal strength in the wireless communication system, ensuring the maintenance of sufficient signal strength for stable connection. The calculation of LM takes into account free-space loss, polarization-matching loss, path loss, shadowing effects, and feeding loss [29]. To guarantee stable transmission in complex environments, LM must always exceed 0 dB. In this research, the proposed antenna operates as a transmitter, while the receiver is suggested to be a dipole antenna [18]. The polarization loss matching value is considered to be 0.6 dB. Furthermore, to avoid interference with adjacent equipment the transmit power of the implanted antenna is constrained to -16 dBm (25μW). All the parameters required for calculating LM are detailed in Table I.

The mathematical representation of the LM is provided as (2).

$$LM = P_a - P_r \tag{2}$$

P_a denotes the energy available from the system, while P_r represents the energy requisite for system operation. The expression of P_r can be represented as (3)

$$P_r(dB) = \frac{E_b}{N_0} + KT_0 + B_r \tag{3}$$

where E_b/N_0 denotes the ratio of bit energy to noise power spectral density which indicates the system's noise tolerance. In this study, this value is set as 9.6 dB. K and T_0 represent the Boltzmann Constant and reference temperature, respectively. The transmission bit rates (B_r) are configured at 1 Mbps, 10 Mbps, 25 Mbps, and 78 Mbps. P_a can be expressed as (4)

$$P_a(dB) = P_t + G_t + G_r - PL - L_p \tag{4}$$

P_t signifies the transmission power limitation of the implanted antenna, G_t denotes the peak gain of the proposed antenna, G_r represents the gain of the external receiving antenna, PL indicates the polarization mismatching loss and L_p corresponds to the path loss which can be represented as

$$L_p(dB) = 20\log_{10}(\frac{4\pi d}{\lambda}) + 10\gamma\log_{10}(\frac{d}{d_0}) + S_e \tag{5}$$

where d is the distance between transmitter and receiver, γ represents the path-loss exponent, and S_e characterizes the shadowing effect, which describes the impact of obstacles on transmission. As illustrated in Fig. 11(a), effective wireless communication links are tested for distances of 7 m, 4 m, 3 m, and 2 m at data rates of 1 Mbps, 10 Mbps, 25 Mbps, and 78 Mbps, respectively, with more than 20 dB margin. This threshold is selected to ensure a more reliable and stable wireless link [28]. Furthermore, considering the high data rate demands of indoor bio-telemetry applications, a range of 5 - 8 meters may be of particular interest [30].

E. MIMO Channel Capacity

Calculating MIMO channel capacity is crucial for WCE applications to ensure reliable data transmission in such challenging environments. MIMO offers significant advantages over Single Input Single Output (SISO) systems by exploiting spatial diversity, increasing data rate, and mitigating multi-path fading effects. Fig. 11(b) shows the channel capacities for different scenarios including SISO ideal, MIMO ideal,

TABLE II
ANTENNA PARAMETERS: COMPARATIVE TABLE WITH THE STATE-OF-THE-ARTS (NM: Not Mention)

Reference	[18]	[31]	[19]	[28]	[32]	**This Work**
Frequency (MHz)	2450	2450	433	915	2450	**915**
FBW (%)	13	16	33.9	12.02	8.5	**84.91**
Antenna Size (λ^3)	6.72×10^{-5}	23.94×10^{-5}	27.6×10^{-5}	0.0256×10^{-5}	7.056×10^{-5}	$\mathbf{0.0468\times10^{-5}}$
Antenna Structure	Planar	Conformal	Planar	Planar	Planar	**Conformal**
System Type	Capsule	Capsule	Capsule/Implantable	Capsule	Implantable	**Capsule**
Elements	2	2	2	2	2	**2**
Isolation (dB)	28	25	26	29	22	**20**
ECC	<0.1	NM	<0.1	<0.1	NM	$\mathbf{<0.1}$
CC@SNR = 20dB(bps/Hz)	9.9	NM	10.2	9.4	NM	$\approx$**14**

and MIMO measured. The measured channel capacity of the proposed model is detailed in [28]. At an SNR of 20 dB, the calculated channel capacities for SISO ideal, MIMO ideal, and MIMO measured are 7.6788, 15.3576, and 13.9349 bits/s/Hz, respectively. Thanks to the ability to exploit spatial diversity, the measured MIMO capacity demonstrates superior performance compared to the theoretically calculated ideal SISO antenna. However, the ideal MIMO capacity outperforms the measured MIMO channel capacity. This is primarily due to the mutual coupling between MIMO antenna elements which is taken into consideration in the experimental measurements.

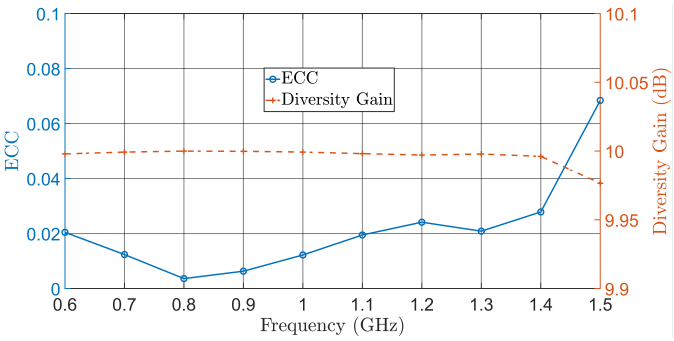

Fig. 12: The ECC and DG at bandwidth.

F. Envelope Correlation Coefficients

In the analysis of MIMO antenna systems, examining the envelope correlation coefficients (ECC) serves as a method for measuring crucial indicators of MIMO systems. This is because ECC effectively captures the correlation between various MIMO channels. In an ideal scenario, the channels of MIMO antennas operate without any interference among themselves, implying an ECC value of 0. However, in practical circumstances, channel interference is inevitable, leading to the conclusion that a lower ECC value is preferable. ECC can be derived from S-parameters and far field radiation patterns gain. The equation for ECC calculation based on S-parameters is presented as (6).

$$ECC = \frac{|S_{11}S_{12}^{*} + S_{21}^{*}S_{22}|}{(1-|S_{11}|^2-|S_{21}|^2)(1-|S_{22}|^2-|S_{12}|^2)} \tag{6}$$

In (6), S_{11} and S_{22} denote the reflection coefficients of antenna 1 and antenna 2, respectively. S_{12} and S_{21} signify the transmission coefficients from antenna 1 to antenna 2 and vice versa. S_{12}^{*} and S_{21}^{*} represent the conjugates of these two parameters. The radiation pattern based formula shows as (7),

$$ECC = \frac{\left|\iint_{4\pi}\left(\vec{An}_i(\theta,\phi)\right)\times\left(\vec{An}_j(\theta,\phi)\right)d\Omega\right|^2}{\iint_{4\pi}\left|\vec{An}_i(\theta,\phi)\right|^2 d\Omega\cdot\iint_{4\pi}\left|\vec{An}_j(\theta,\phi)\right|^2 d\Omega} \tag{7}$$

where $\vec{An}_i(\theta,\phi)$ and $\vec{An}_j(\theta,\phi)$ are 3-D radiation pattern of Antenna-1 and Antenna-2 and Ω represents the solid angle. To assess the signal quality and reliability of MIMO antennas, the concept of diversity gain (DG) is utilized to evaluate the enhancement in antenna system performance. The DG can be calculated as (8)

$$DG = 10\sqrt{1-(ECC)^2} \tag{8}$$

The ECC and DG are presented in Fig. 12, Within the antenna's operating frequency range, the acquired ECC value is below 0.1, and the DG value exceeds 9.9 dB.

A comparative analysis of current research and the proposed work is presented in Table II. Relative to existing work, the model introduced in this study not only boasts a more compact geometric structure but also stands out as the sole design featuring ultra-bandwidth characteristics among MIMO designs. Additionally, compared with other studies, this model exhibits a higher channel capacity due to its ultra-wide bandwidth. Moreover, it can effectively mitigate frequency detuning offered by the heterogeneous GI tract.

IV. Conclusion

An implantable MIMO antenna for a minimal-sized capsule endoscope is proposed, including design, optimization, simulation, and measurement phases. The suggested MIMO antenna is positioned in the upper and lower sections of the capsule, each stimulated by independent ports. It exhibits ultra-bandwidth characteristics at the designated operating frequency. Moreover, utilizing multiple folding techniques and a meandering structure, the proposed antenna achieves a compact size of 30.5 mm $\times$ 15 mm $\times$ 0.04 mm, resulting

in a volume of 18.3 mm^3. holes are positioned between the two antennas to improve impedance matching. This design approach ultimately achieves an FBW of 84.91% and an isolation of 20 dB. The calculated ECC falls below 0.1, the DG exceeds 9.9 dB, and the channel capacity reaches 14 bps/Hz at an SNR of 20 dB. Consequently, the MIMO antenna model proposed in this study emerges as an outstanding choice to facilitate the frequency detuning and high channel capacity requirements for transmitting high-resolution images.

REFERENCES

[1] G. Iddan, G. Meron, A. Glukhovsky, and P. Swain, "Wireless capsule endoscopy," *Nature*, vol. 405, no. 6785, pp. 417–417, 2000.

[2] M. Zada, I. A. Shah, A. Basir, and H. Yoo, "Ultra-compact implantable antenna with enhanced performance for leadless cardiac pacemaker system," *IEEE Transactions on Antennas and Propagation*, vol. 69, no. 2, pp. 1152–1157, 2021.

[3] S. A. A. Shah and H. Yoo, "Scalp-implantable antenna systems for intracranial pressure monitoring," *IEEE Transactions on Antennas and Propagation*, vol. 66, no. 4, pp. 2170–2173, 2018.

[4] W. Khan, E. Muntimadugu, M. Jaffe, and A. J. Domb, "Implantable medical devices," *Focal controlled drug delivery*, pp. 33–59, 2014.

[5] Y. Wang, B. Huang, and S. Yan, "A conformal four-antenna module for capsule endoscope mimo operation," *IEEE Transactions on Antennas and Propagation*, vol. 70, no. 11, pp. 10 270–10 285, 2022.

[6] J. Shang and Y. Yu, "An ultrawideband capsule antenna for biomedical applications," *IEEE Antennas and Wireless Propagation Letters*, vol. 18, no. 12, pp. 2548–2551, 2019.

[7] K. Liu, R. Liu, W. Cui, K. Zhang, M. Wang, C. Fan, H. Zheng, and E. Li, "Design of conformal spiral dual-band antenna for wireless capsule system," *IEEE Access*, vol. 9, pp. 117 349–117 357, 2021.

[8] J. Shang and Y. Yu, "An ultrawideband and conformal antenna for wireless capsule endoscopy," *Microwave and Optical Technology Letters*, vol. 62, no. 2, pp. 860–865, 2020.

[9] Y. A. Salchak, N. M. Albadri, M. T. Worsey, H. G. Espinosa, and D. V. Thiel, "Surface electric field variations due to different human postures for wireless endoscopy applications," *IEEE Transactions on Instrumentation and Measurement*, vol. 70, pp. 1–11, 2021.

[10] R. Das and H. Yoo, "A wideband circularly polarized conformal endoscopic antenna system for high-speed data transfer," *IEEE Transactions on Antennas and Propagation*, vol. 65, no. 6, pp. 2816–2826, 2017.

[11] K. Zhang, C. Liu, X. Liu, H. Cao, Y. Zhang, X. Yang, and H. Guo, "A conformal differentially fed antenna for ingestible capsule system," *IEEE Transactions on Antennas and Propagation*, vol. 66, no. 4, pp. 1695–1703, 2018.

[12] W. Lei and Y.-X. Guo, "Design of a dual-polarized wideband conformal loop antenna for capsule endoscopy systems," *IEEE Transactions on Antennas and Propagation*, vol. 66, no. 11, pp. 5706–5715, 2018.

[13] H. Q. Ngo, E. G. Larsson, and T. L. Marzetta, "Energy and spectral efficiency of very large multiuser mimo systems," *IEEE Transactions on Communications*, vol. 61, no. 4, pp. 1436–1449, 2013.

[14] M. Suzan Miah, A. N. Khan, C. Icheln, K. Haneda, and K.-I. Takizawa, "Antenna system design for improved wireless capsule endoscope links at 433 mhz," *IEEE Transactions on Antennas and Propagation*, vol. 67, no. 4, pp. 2687–2699, 2019.

[15] E. Cil, I. V. Soares, D. Renaudeau, R. Lucas, S. Dumanli, R. Sauleau, and D. Nikolayev, "On the use of impedance detuning for gastrointestinal segment tracking of ingestible capsules," *IEEE Transactions on Antennas and Propagation*, vol. 71, no. 2, pp. 1977–1981, 2023.

[16] J. Wang, M. Leach, E. G. Lim, Z. Wang, R. Pei, and Y. Huang, "An implantable and conformal antenna for wireless capsule endoscopy," *IEEE Antennas and Wireless Propagation Letters*, vol. 17, no. 7, pp. 1153–1157, 2018.

[17] M. S. Sharawi, "Current misuses and future prospects for printed multiple-input, multiple-output antenna systems [wireless corner]," *IEEE Antennas and Propagation Magazine*, vol. 59, no. 2, pp. 162–170, 2017.

[18] A. J. Alazemi and A. Iqbal, "A high data rate implantable mimo antenna for deep implanted biomedical devices," *IEEE Transactions on Antennas and Propagation*, vol. 70, no. 2, pp. 998–1007, 2022.

[19] A. Iqbal, M. Al-Hasan, I. B. Mabrouk, and M. Nedil, "A compact implantable mimo antenna for high-data-rate biotelemetry applications," *IEEE Transactions on Antennas and Propagation*, vol. 70, no. 1, pp. 631–640, 2022.

[20] S. Xiao, C. Liu, Y. Li, X. M. Yang, and X. Liu, "Small-size dual-antenna implantable system for biotelemetry devices," *IEEE Antennas and Wireless Propagation Letters*, vol. 15, pp. 1723–1726, 2016.

[21] A. Iqbal, M. Al-Hasan, I. B. Mabrouk, and M. Nedil, "Scalp-implantable mimo antenna for high-data-rate head implants," *IEEE Antennas and Wireless Propagation Letters*, vol. 20, no. 12, pp. 2529–2533, 2021.

[22] K. Liu, Z. Li, W. Cui, K. Zhang, M. Wang, C. Fan, H. Zheng, and E. Li, "Investigation of conformal mimo antenna for implantable devices based on theory of characteristic modes," *IEEE Transactions on Antennas and Propagation*, vol. 70, no. 12, pp. 11 324–11 334, 2022.

[23] Y. Wang, B. Huang, and S. Yan, "A conformal four-antenna module for capsule endoscope mimo operation," *IEEE Transactions on Antennas and Propagation*, vol. 70, no. 11, pp. 10 270–10 285, 2022.

[24] G. Gauthier, A. Courtay, and G. Rebeiz, "Microstrip antennas on synthesized low dielectric-constant substrates," *IEEE Transactions on Antennas and Propagation*, vol. 45, no. 8, pp. 1310–1314, 1997.

[25] C. Gabriel, S. Gabriel, and E. Corthout, "The dielectric properties of biological tissues: I. literature survey," *Physics in Medicine Biology*, vol. 41, no. 11, p. 2231, nov 1996. [Online]. Available: https://dx.doi.org/10.1088/0031-9155/41/11/001

[26] C. Xiao, S. Hao, and Y. Zhang, "915 mhz miniaturized loop conformal antenna for capsule endoscope," *IEEE Transactions on Antennas and Propagation*, vol. 70, no. 11, pp. 10 233–10 244, 2022.

[27] "Ieee standard for safety levels with respect to human exposure to electric, magnetic, and electromagnetic fields, 0 hz to 300 ghz," *IEEE Std C95.1-2019 (Revision of IEEE Std C95.1-2005/ Incorporates IEEE Std C95.1-2019/Cor 1-2019)*, pp. 1–312, 2019.

[28] A. Iqbal, M. Al-Hasan, I. B. Mabrouk, and T. A. Denidni, "Capsule endoscopic mimo antenna with radiation pattern and polarization diversity," *IEEE Transactions on Antennas and Propagation*, vol. 71, no. 4, pp. 3146–3154, 2023.

[29] I. Gani and H. Yoo, "Multi-band antenna system for skin implant," *IEEE Microwave and Wireless Components Letters*, vol. 26, no. 4, pp. 294–296, 2016.

[30] A. Basir, M. Zada, Y. Cho, and H. Yoo, "A dual-circular-polarized endoscopic antenna with wideband characteristics and wireless biotelemetric link characterization," *IEEE Transactions on Antennas and Propagation*, vol. 68, no. 10, pp. 6953–6963, 2020.

[31] L.-J. Xu, B. Li, M. Zhang, and Y. Bo, "Conformal mimo loop antenna for ingestible capsule applications," *Electronics Letters*, vol. 53, no. 23, pp. 1506–1508, 2017.

[32] M. S. Singh, J. Ghosh, S. Ghosh, and A. Sarkhel, "Miniaturized dual-antenna system for implantable biotelemetry application," *IEEE Antennas and Wireless Propagation Letters*, vol. 20, no. 8, pp. 1394–1398, 2021.

Liu Chang (Student Member, IEEE)received the B.A.Sc. degrees in Computer Science from the Macau University of Science and Technology, Macau, China, in 2020, and received M.A.Sc. degree in Electrical and Electronic Engineering from Durham University, Durham, England, UK, in 2022. He is currently pursuing the Ph.D degree in Electrical and Electronic Engineering in Durham University, Durham, England, UK. His research interests include wireless capsule endoscopy, antenna, implantable medical devices.

Amjad Iqbal (Member, IEEE) received the B.S. degree in electrical engineering from COMSATS University, Islamabad, Pakistan, in 2016, the M.S. degree in electrical engineering from the CECOS University of IT and Emerging Sciences, Peshawar, Pakistan, in 2018, and the Ph.D. degree in engineering from Multimedia University, Selangor, Malaysia, in 2021.

He worked as a Laboratory Engineer with the Department of Electrical Engineering, CECOS University Peshawar, Peshawar, from 2016 to 2018. His research interests include printed antennas, flexible antennas, implantable antennas, multiple-input and multiple-output (MIMO) antennas, dielectric resonator antennas, wireless power transfer, and synthesis of microwave components.

Abdul Basir] (Member, IEEE) is born in Khyber Pakhtunkhwa, Pakistan, in 1989. He earned his B.Sc. degree in Telecommunication Engineering from the University of Engineering and Technology, Peshawar, Pakistan, in 2015. Driven by a passion for research, he pursued and successfully attained a Ph.D. degree in Electronic Engineering from Hanyang University, Seoul, South Korea, in 2021.

Dr. Basir worked as a postdoctoral researcher at Applied Bioelectronics Laboratory Korea from September 2021 to 2024. Currently, he is contributing significantly to the academic and research community as a Postdoctoral Research Fellow at Tampere University, Finland. In this role, he continues to advance knowledge in electronic and biomedical engineering, exploring diverse areas such as implantable antennas and systems, biomedical circuits, wearable antennas, MIMO communication, metamaterials, dielectric resonator antennas, reconfigurable antennas, long-range wireless power transfer, and wireless charging of biomedical implants.

Dr. Basir's commitment to academic excellence extends beyond his research pursuits. He is a prolific reviewer, contributing to the peer-review process for over 200 activities across esteemed journals such as IEEE Transactions on Antenna and Propagation, Advanced Material Technologies, IEEE AWPL, Electronics Letters, Frontier of Information Technology and Electronic Engineering, IEEE Access, IEEE Internet of Things Journal, IEEE Journal of Biomedical and Health Informatics, and more.

In recognition of his outstanding contributions, Dr. Basir has received several prestigious awards, including the Silver Prize for the Best Student Paper Awards in Student Paper Contests from IEEE Seoul Section in 2018 and 2019. Additionally, a collaborative paper under his involvement received the Best Paper Award in 2019 from the IEEE AP/MTT/EMC Joint Chapter Malaysia. His dedication to excellence is further underscored by the Third Prize for the Best Student Paper Competition in 2018 by the Korea Communications Agency (KCA) and the Korean Institute of Electromagnetic Engineering and Science (KIEES).

Dr. Basir's role as a Postdoctoral Research Fellow at Tampere University positions him as a valuable contributor to the global research landscape, emphasizing his commitment to advancing knowledge and shaping the future of bioelectronics and biomedical engineering.

Roy B. V. B. Simorangkir (Member, IEEE) holds a B.S. degree in Telecommunication Engineering from the Institut Teknologi Bandung, Indonesia (2010), an M.S. degree in Electrical and Electronic Engineering from Yonsei University, South Korea (2014), and a Ph.D. in Electronic Engineering from Macquarie University, Australia (2018). After completing his Ph.D., he pursued postdoctoral research at Macquarie University, Institute of Electronics and Telecommunications of Rennes, France, and Tyndall National Institute, Ireland. Dr. Simorangkir is currently an Assistant Professor in the Department of Engineering at Durham University, UK, where he specializes in the development of unconventional materials-based antennas and sensors for next-generation wireless communication and sensing systems. He has published over 60 refereed research papers in this field, including award-winning work. He has also taken on leadership roles at major international conferences and received recognition as an outstanding reviewer for esteemed journals, notably from 2021 to 2023 for the IEEE Transactions on Antennas and Propagation

Ismail Ben Mabrouk (Senior Member, IEEE) received the B.A.Sc. and M.A.Sc. degrees in electrical engineering from the University of Lille, Lille, France, in 2006 and 2007, respectively, and the Ph.D. degree in electrical engineering from the University of Quebec, Montreal, QC, Canada, in 2012.

From 2007 to 2009, he is with Huawei Technologies, Paris, France. In 2012, he joined the Wireless Devices and Systems (WiDeS) Group, University of Southern California, Los Angeles, CA, USA. He is currently an Assistant Professor with Durham University, Durham, U.K. His research activities have been centered on antenna design at the millimeter-wave and THz frequencies, propagation studies for multiple-input and multiple-output (MIMO) systems, deep learning, and wireless body area network for medical applications.

Dr. Mabrouk is a recipient of the Abu Dhabi Award for Research Excellence (AARE) in 2018.